Tau/QED-07/09

BAD 2222, version 6

Collaboration-Wide Review

11 July 2009 to 22 July 2009

Primary BAD	2222, version 6 `Analysis of the tau->KsPinu mass spectrum, and measurement of tau->KsPinu and tau->KsPiPi0nu branching fractions.`
Author list	Banerjee, Swagato; Cowan, Glen; Paramesvaran, Sudarshan
Review Committee	comm392, members: Barlow, Roger; Nugent, Ian M.; Sekula, Stephen J. (chair)
Target	
Result type	
Supporting BAD(s)	BAD #2055 `Analysis of the tau-> Ks Pi nu invariant mass spectrum using the BaBar detector`
Changes since preliminary result	`This result performs a fit to the mass spectrum of the Ks pi system and measures the K* mass and width, as well as looking for evidence of other resonance contributions to the spectrum.`
BAIS/CWR Comments	`This resulted is aimed for physics sign-off in time for presentation at DPF and any other following summer conference.  A separate and full publication of these results will follow this preliminary result of the fits to the mass spectrum.`
Institutional Reading Groups	2b. Budker, UCLA, Colorado, Royal Holloway, McGill, MIT, Trieste

Cover page generated by BAIS on July 11, 2009

Analysis of the decays $\tau^- \to K_S^0\pi^-\nu_\tau$ and $\tau^- \to K_S^0\pi^-\pi^0\nu_\tau$ using the *BABAR* detector

The *BABAR* Collaboration

July 11, 2009

Abstract

We present studies of the decays $\tau^- \to K_S^0\pi^-\nu_\tau$ and $\tau^- \to K_S^0\pi^-\pi^0\nu_\tau$ using $384.6\,\mathrm{fb}^{-1}$ of e^+e^- collision data provided by the PEP-II accelerator, operating primarily at $\sqrt{s} = 10.58\,\mathrm{GeV}$, and recorded using the *BABAR* detector. For $\tau^- \to K_S^0\pi^-\nu_\tau$ we carry out a fit to the hadronic mass distribution which yields values for the K*(892) mass and width:

$$M(K^*(892)^-) = 894.30 \pm 0.19\,(\mathrm{stat.}) \pm 0.19\,(\mathrm{syst.})\,\mathrm{MeV}\,,$$
$$\Gamma(K^*(892)^-) = 45.56 \pm 0.43\,(\mathrm{stat.}) \pm 0.57\,(\mathrm{syst.})\,\mathrm{MeV}\,.$$

We analyse the possiblity of other resonances being present in this mass spectrum, and conclude that a combination of K*(800), K*(892) and K*(1410) provides a good description of the data. A fit without the K*(800), i.e., using only a K*(892) + K*(1410) combination, can also provide a good description of the data if the modeling of backgrounds were to be incorrect by a significant amount. Studies are presented which consider how the principal background mode must be altered for a two-resonance model to fit the data. The altered background model is reasonably consistent, within experimental uncertainty, to the data used for the Monte Carlo generation of this background. It is therefore not possible at this moment to confirm the necessity of a K*(800) resonance to fit the $\tau^- \to K_S^0\pi^-\nu_\tau$ invariant mass spectrum.

In addition we have studied the hadronic mass distribution for the decay $\tau^- \to K_S^0\pi^-\pi^0\nu_\tau$. The measurement is used to improve the Monte Carlo simulation of this decay, which was needed for a background estimate in the analysis of the $K_S^0\pi^-\nu_\tau$ mode. The branching ratio for $\tau^- \to K^0\pi^-\pi^0\nu_\tau$ is measured to be

$$\mathcal{B}(\tau^- \to K^0\pi^-\pi^0\nu_\tau) = (0.342 \pm 0.006\,(\mathrm{stat.}) \pm 0.015\,(\mathrm{sys.}))\%\,.$$

SLAC NAtional Accelerator Laboratory, Stanford University, Stanford, CA 94309

Work supported in part by Department of Energy contract DE-AC02-76SF00515.

1 INTRODUCTION

Studies are presented of the hadronic mass distributions for the decays $\tau^- \to K^0_S\pi^-\nu_\tau$ and $\tau^- \to K^0_S\pi^-\pi^0\nu_\tau$ (throughout the note, charge conjugate modes are included).

Since the 2008 [1] analysis, important improvements have been carried out in the modeling of the background in that mode from $\tau^- \to K^0_S\pi^-\pi^0\nu_\tau$, which are presented here. The measurements have been used to tune the `TAUOLA` Monte Carlo model [2] used to describe the τ-lepton decay. This is then used to model the background from $K^0_S\pi^-\pi^0\nu_\tau$ in the analysis of $\tau^- \to K^0_S\pi^-\nu_\tau$. The resulting branching ratio for $\tau^- \to K^0_S\pi^-\nu_\tau$ is fully consistent with the 2008 preliminary value.

For the decay $\tau^- \to K^0_S\pi^-\nu_\tau$ we carry out a fit of the hadronic mass distribution that yields precise values for the mass and width of the K*(892) as well as information on other resonances present in the distribution. The Belle collaboration recently published [3] an analysis of the hadronic mass distribution for this mode, where they quoted measurements of the K*(892) mass and width in significant disagreement with the values determined by the PDG [8].

It is known that the K*(892) provides the main contribution to the $K\pi$ mass spectrum, but prior to the Belle measurement there had been no definitive evidence for additional resonances (e.g., scalar or tensor contributions). Although these are expected theoretically, the large data sample required to perform a detailed study had not been available. Belle has proposed the mass distribution should contain a contribution from a scalar meson at 800 MeV, as without it they cannot sufficiently describe the low end of the spectrum.

The event selection for the $K^0_S\pi^-\nu_\tau$ mode is described in Ref. [1], where details are also given about the data and Monte Carlo samples used. For the $K^0_S\pi^-\pi^0\nu_\tau$ final state we begin with the same selection criteria but then include an additional π^0, as described in Section 3.1.

The analysis of $K^0_S\pi^-\pi^0\nu_\tau$ is described in Section 4. This includes both the measurement of the branching ratio and the use of the observed mass distribution to improve the `TAUOLA` Monte Carlo generator.

The analysis of the hadronic mass distribution for the $\tau^- \to K^0_S\pi^-\nu_\tau$ final state is described in Section 5, the fit results are presented in Section 5.5, and the systematic uncertainties are discussed in Section 5.6. The results are summarized and conclusions given in Sections 5.5 and 6.

2 THE *BABAR* DETECTOR AND DATASET

The *BABAR* detector is described in detail in Ref [4]. Charged particles are detected and their momenta measured with a 5-layer double sided silicon vertex tracker (SVT) and a 40-layer drift chamber (DCH) inside a 1.5 T superconducting solenoidal magnet. A ring-imaging Cherenkov detector (DIRC) is used for the identification of charged particles. Energies of neutral particles are measured by an electromagnetic calorimeter (EMC) composed of 6,580 CsI(Tl) crystals,and the instrumented magnetic flux return (IFR) is used to identify muons.

The analysis described in this paper is based on data taken using the *BABAR* detector at the PEP-II collider [5] located at the SLAC National Accelerator Laboratory in the data-taking periods between October 1999 and August 2006. During this period a total of $384.6\,\mathrm{fb}^{-1}$ of data was recorded with a cross-section for $\tau^+\tau^-$ pair production of $(0.919 \pm 0.003)\,\mathrm{nb}$ [6]. This data sample contains over 700 million τ decays.

Monte Carlo (MC) studies of simulated signal and background events were carried out using various MC samples. The τ MC events studied were generated with `KK2f` [7] and decayed with `TAUOLA` [2] using τ branching fractions based on Ref [8]. In the MC, the τ^- decays to $K^0_S\pi^-$ via the $K^*(892)^-$ resonance with a branching fraction of 0.90%. Non-τ hadronic and dilepton MC samples are used for studying the non-τ backgrounds.

Important improvements to TAUOLA's modeling of the decay $\tau^- \rightarrow K_S^0\pi^-\pi^0\nu_\tau$ were undertaken as part of this analysis, as described in Section 4.

3 EVENT SELECTION

The analysis uses $384.6\,\mathrm{fb}^{-1}$ of data taken between October 1999 and August 2006 (runs 1 through 5). The event selection for $\tau^- \rightarrow K_S^0\pi^-\nu_\tau$ is described in Ref. [1]. For $\tau^- \rightarrow K_S^0\pi^-\pi^0\nu_\tau$ one begins with the same selection as for $K_S^0\pi^-\nu_\tau$ and then requires an additional π^0, which is described in Section 3.1.

3.1 EVENT SELECTION FOR $\tau^- \rightarrow K_S^0\pi^-\pi^0\nu_\tau$

Using the selection criteria in the analysis of $\tau^- \rightarrow K_S^0\pi^-\nu_\tau$ as a starting point, we then made the following adjustments to select events for $\tau^- \rightarrow K_S^0\pi^-\pi^0\nu_\tau$. We require:

- exactly one identified π^0 in the event;
- the trajectory of the π^0 must be within 90 degrees of the $K_S^0\pi^-$ momentum vector. This ensures that the π^0 is more likely to be from the same τ as the $K_s\pi$;
- the neutral energy not attributed to the K_S^0 or the π^0 must be less then 100 MeV. This should be very small anyway, but the cut is to reject unwanted photons;
- the energy of the π^0 in the center-of-mass system must be greater than 1.2 GeV. This cut is to remove the large background contribution in the region below 1.2 GeV.

As an example, Fig. 1 shows the distribution of the π^0 energy. The combination of all cuts results in a signal efficiency of 0.500% with a purity of 93%; more details are given in Section 4.

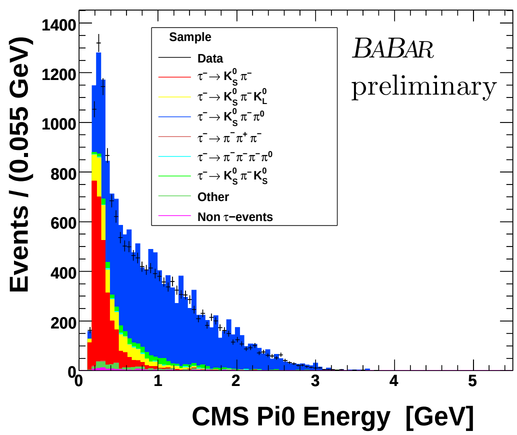

Figure 1: Distribution of the π^0 energy.

4 ANALYSIS OF $\tau^- \to K^0_S\pi^-\pi^0\nu_\tau$

For the decay mode $\tau^- \to K^0_S\pi^-\pi^0\nu_\tau$ we have measured the branching ratio, which is described in Section 4.1, and we also carry out an analysis of the hadronic mass distribution, shown in Section 4.2.

4.1 Branching fraction measurement

Defining the signal process to be $\tau^\pm \to K^0_S\pi^\pm\pi^0\nu_\tau$ with $K^0_S \to \pi^+\pi^-$, our overall signal efficiency is found to be

$$\varepsilon_{\rm sig} = \frac{N^{\rm sel}_{\rm sig}}{N^{\rm gen}_{\rm sig}} = 0.00500 \pm 0.00008\,({\rm stat.})\ . \tag{1}$$

Redefining the signal process to be $\tau^- \to \bar{K}^0\pi^-\pi^0\nu_\tau$, the signal efficiency becomes $\varepsilon^{'}_{\rm sig} = \varepsilon_{\rm sig} \times \mathcal{B}(\bar{K}^0 = K^0_S) \times \mathcal{B}(K^0_S \to \pi^+\pi^-)$. The branching fraction $\mathcal{B}(\tau^- \to \bar{K}^0\pi^-\pi^0\nu_\tau)$ is estimated by

$$\mathcal{B}(\tau^- \to \bar{K}^0\pi^-\pi^0\nu_\tau) = \frac{1}{2N_{\tau\tau}}\frac{N_{\rm data} - N_{\rm bkg}}{\varepsilon^{'}_{\rm sig}}, \tag{2}$$

where $N_{\tau\tau}$ is the total number of $\tau^+\tau^-$ pairs in the real data, $N_{\rm data}$ is the number of selected events in real data, $N_{\rm bkg}$ is the number of background events estimated from Monte Carlo.

Table 1: $\mathcal{B}(\tau^- \to \bar{K}^0\pi^-\pi^0\nu_\tau)$ measured in this analysis.

Sample	$\mathcal{B}(\tau^- \to \bar{K}^0\pi^-\pi^0\nu_\tau)$ [%]
e-tag	$0.353 \pm 0.008\,({\rm stat}) \pm 0.016\,({\rm syst})$
μ-tag	$0.329 \pm 0.008\,({\rm stat}) \pm 0.016\,({\rm syst})$
Combined	$0.342 \pm 0.006\,({\rm stat}) \pm 0.015\,({\rm syst})$

Most of the systematic uncertainties related to this measurement are common to those of the original $\tau^- \to \bar{K}^0\pi^-\nu_\tau$ analysis, details of which are given in Ref. [1]. In addition to the uncertainties included from the $\tau^- \to \bar{K}^0\pi^-\nu_\tau$ analysis, a 3% systematic for the π^0 efficiency correction was added in quadrature. A summary of the systematic uncertainties is given on the next page. It has been checked that the effect on the estimated branching fraction of varying the cut on the π^0 energy is small compared to the quoted systematic uncertainty.

4.2 Hadronic mass distributions for $\tau^- \to K^0_S\pi^-\pi^0\nu_\tau$

Figure 2 shows the hadronic mass distributions from the $\tau^- \to K^0_S\pi^-\pi^0\nu_\tau$ decays for different combinations of the final state hadrons: $\pi^-\pi^0$, $K^0_S\pi^-$, $K^0_S\pi^0$ and $K^0_S\pi^-\pi^0$. The plots show the observed distributions (data points), and Monte Carlo predictions for signal (blue) and background. The signal predictions are based on the original `TAUOLA` generator and show large discrepancies with the measurements. Figure 2(b) shows specifically how the signal Monte Carlo had no K*(892) resonance, while our data clearly exhibit this peak.

The measured distributions were used to improve the form factors in the `TAUOLA` generator leading to a greatly improved description of the $\tau^- \to K^0_S\pi^-\pi^0$ decay. Figure 3 shows the background subtracted measurements for the same mass combinations as in Fig. 2 along with both the old and

Table 2: Summary of the systematic uncertainties as they feed into the measurement of $\mathcal{B}(\tau^- \to K^0\pi^-\pi^0\nu_\tau)$.

Systematic	e-tag	μ-tag	Combined
Tracking	0.58%	0.58%	0.58%
K_S^0 Efficiency	1.40%	1.40%	1.40%
PID	1.45%	1.68%	1.50%
$\mathcal{L} \times \sigma_{\tau\tau}$	0.70%	0.70%	0.70%
MC signal	1.87%	2.08%	1.39%
MC background	0.28%	0.30%	0.20%
τ backgrounds	1.37%	1.37%	1.37%
Modelling	0.37%	0.37%	0.37%
π^0 efficiency	3.30%	3.30%	3.30%
Total	4.55%	4.77%	4.41%

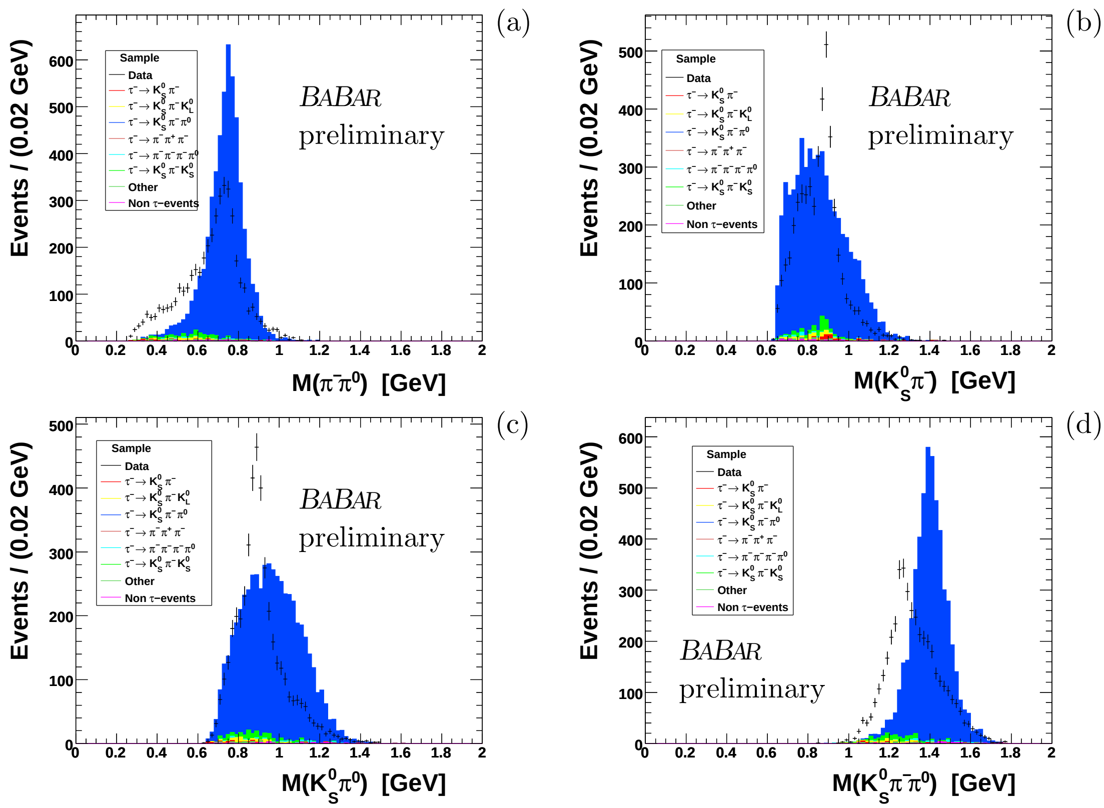

Figure 2: Invariant mass distributions of different hadron combinations from the $K_S^0\pi^-\pi^0$ final state showing data (points) and MC predictions for background and signal (in blue) based on the original version of `TAUOLA`: (a) $\pi^-\pi^0$, (b)$K_S^0\pi^-$, (c) $K_S^0\pi^0$ and (d) $K_S^0\pi^-\pi^0$. The overall normalization of the MC predictions is scaled to be the same as that of the data.

improved Monte Carlo predictions. This new Monte Carlo is used to determine the efficiency for our measurement of the $\tau^- \to K_S^0\pi^-\pi^0$ branching ratio described above, and it is also used in our analysis of the $\tau^- \to K_S^0\pi^-\nu_\tau$ mass spectrum.

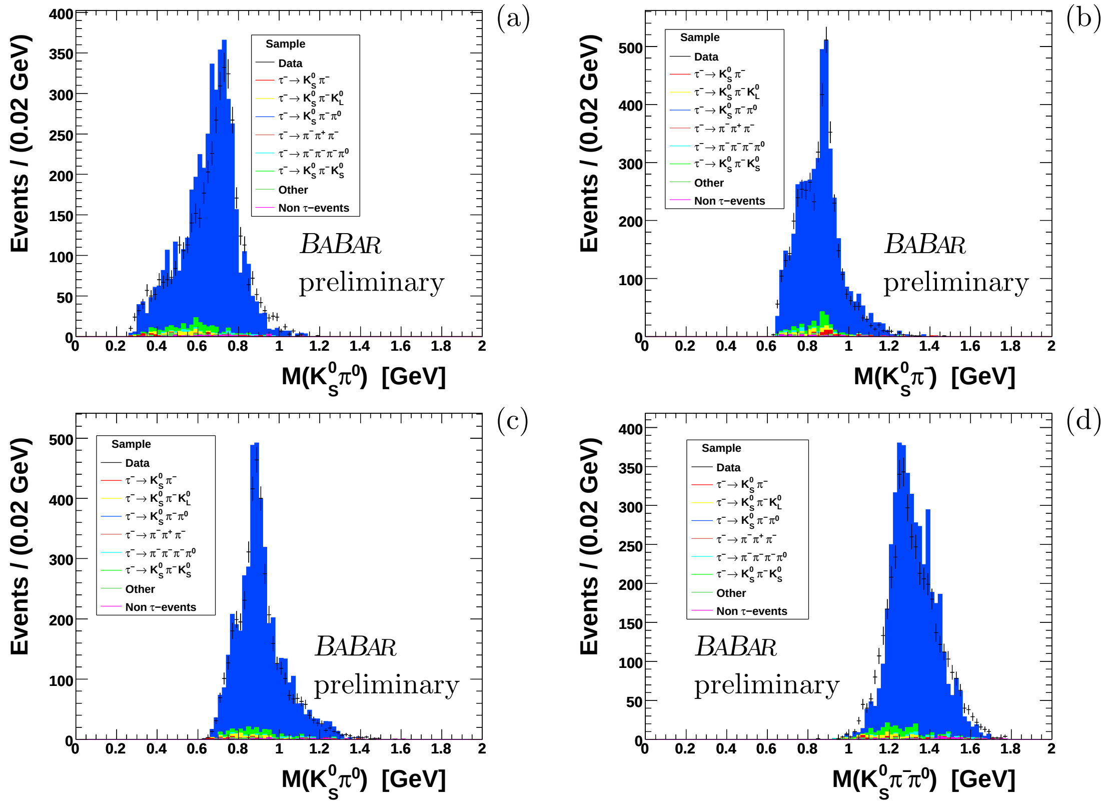

Figure 3: Invariant mass distributions of different hadron combinations from the $K_S^0\pi^-\pi^0$ final state showing data (points) MC predictions for background and signal (in blue) based on the tuned version of `TAUOLA`: (a) $\pi^-\pi^0$, (b)$K_S^0\pi^-$, (c) $K_S^0\pi^0$ and (d) $K_S^0\pi^-\pi^0$. The overall normalization of the MC predictions is scaled to be the same as that of the data.

5 ANALYSIS OF $\tau^- \to K_S^0\pi^-\nu_\tau$

The analysis of the decay $\tau^- \to K_S^0\pi^-\nu_\tau$ is a fit of the hadronic mass distribution to a parametric function describing the resonant structure. From this we obtain precise values for the mass and width of the K*(892) as well as information on other resonances present in the spectrum.

5.1 Fit methodology and signal model

We denote the number of events found in bin i (without background subtraction) by n_i. The prediction for the expectation value of n_i, $\nu_i = E[n_i]$, can be written

$$\nu_i = \sum_{j=1}^{M} R_{ij}\mu_j + \beta_i \; , \tag{3}$$

where β_i is the number of background events, μ_j is the predicted number of signal events in bin j before detector effects (the "true" distribution), and R_{ij} is a response matrix that reflects the limited efficiency and resolution of the detector. The value of R_{ij} is the probability for a signal event created in bin j to be found in bin i,

$$R_{ij} = P(\text{event found in bin } i \,|\text{event created in bin } j) \; , \tag{4}$$

and thus the efficiency for bin j is found by summing over all bins where the event could be found, i.e.,

$$\varepsilon_j = \sum_{i=1}^{N} R_{ij} = P(\text{event found anywhere}|\text{event created in bin } j) \; . \tag{5}$$

The predicted number of events in bin j of the true distribution can be written

$$\mu_j = \mu_{\text{tot}} \int_{\text{bin}\, i} f(m;\vec{\theta})\, dm \; , \tag{6}$$

where m denotes the $K^0_S\pi^-$ invariant mass and $\vec{\theta}$ represents a set of parameters. When calculating the value of the signal pdf in each bin, a numerical integration should be performed over the bin width. Where the bin width is small, however, it is a good approximation to take the pdf's value in the centre of the bin and multiply by the bin width. This is done except in the regions where the distribution is varying rapidly, i.e., near the K*(892) peak and also just above the kinematic threshold.

The probability density function (pdf) $f(m;\vec{\theta})$ can be written

$$f(m;\vec{\theta}) \propto \frac{1}{s}\left(1 - \frac{s}{{m_\tau}^2}\right)\left(1 + 2\frac{s}{{m_\tau}^2}\right) P \left(P^2|F_V|^2 + \frac{3({m_K}^2 - {m_\pi}^2)^2}{4s(1 + 2\frac{s}{{m_\tau}^2})}|F_S|^2\right) . \tag{7}$$

where $s = m^2$. Here the vector form factor F_V is given by

$$F_V = \frac{1}{1 + \beta + \gamma + \cdots}[BW_{K^1}(s) + \beta BW_{K^2}(s) + \gamma BW_{K^3}(s) + \cdots] \; . \tag{8}$$

This form allows for the K*(892) and two additional vector resonances. The quantities β and γ are complex interference terms between the resonances, and the BW terms refer to the to relativistic Breit-Wigner functions for the specific resonance, given by

$$BW_R(s) = \frac{M_R^2}{s - M_R^2 + i\sqrt{s}\Gamma_R(s)} \; . \tag{9}$$

The energy dependent width is given by

$$\Gamma_R(s) = \Gamma_0 R \frac{M_R^2}{s}\left(\frac{P(s)}{P(M_R^2)}\right)^{2\ell+1} \; , \tag{10}$$

where

$$P(s) = \frac{1}{2\sqrt{s}}\sqrt{(s-M_+^2)(s-M_-^2)}\ , \tag{11}$$

and where $M_- = M_K - M_\pi$, $M_+ = M_K + M_\pi$, and ℓ is orbital angular momentum. Thus one has $\ell = 1$ if the $K\pi$ system is from a P-wave (vector), or $\ell = 0$ if the $K\pi$ system is from an S-wave (scalar).

The scalar form factor requires a different parametric function and can include contributions from the K*(800) and K*(1430) signals. This is

$$F_S = \varkappa \frac{s}{M^2_{K*(800)}} BW_{K*(800)}(s) + \lambda \frac{s}{M^2_{K*(1430)}} BW_{K*(1430)}(s)\ . \tag{12}$$

We have also investigated using the LASS function for the scalar contribution, which is given by (see Ref. [10])

$$F_S = \lambda A_s, A_s = \frac{\sqrt{s}}{P}(\sin\delta_B e^{i\delta_B} + e^{2i\delta_B} BW_{K*(1430)})\ , \tag{13}$$

where λ is a real constant, and P is defined in Eq. 11. The phase δ_B is defined by the equation:

$$\cot\delta_B = \frac{1}{aP} + \frac{bP}{2} \tag{14}$$

As will be shown below, the description of the data when using the LASS function is significantly worse than when using Eq. 12.

5.2 Response matrix

To predict the number of entries in each bin of the observed mass distribution one requires the response matrix R_{ij}, which reflects the limited efficiency and resolution of the detector. This is obtained from the Monte Carlo, which we use to produce a two-dimensional distribution of the measured minus true hadronic mass,

$$x = m_{\text{meas}} - m_{\text{true}}\ , \tag{15}$$

versus the true mass. We then split the distribution into vertical slices and project onto the vertical (measured minus true mass) axis. These distributions represent the detector response corresponding to the true mass of each slice. The distributions from each slice were fitted with a parametric pdf, and the resulting parameters were themselves parametrized as a function of the true mass. The slices were chosen such that all of the projected distributions have approximately the same number of events to avoid spurious fit results due to extremely small numbers of events.

The tails of the distributions of $x = m_{\text{meas}} - m_{\text{true}}$ were seen to be longer than those which a Gaussian pdf could accurately fit, but a good description was obtained with a Student's t distribution,

$$f(x;\mu,\lambda,\nu) = \frac{1}{\lambda}\frac{\Gamma((\nu+1)/2)}{\sqrt{\nu\pi}\Gamma(\nu/2)}\left(1+\frac{t^2}{\nu}\right)^{-(\nu+1)/2}\ , \tag{16}$$

where

$$t = \frac{x-\mu}{\lambda}\ . \tag{17}$$

The Student's t distribution is flexible enough to account for the long tails because of its parameter ν, which in effect controls the extent of the tails. As ν goes to infinity the tail approaches Gaussian form, and if ν is 1, then the tail is that of a Cauchy distribution.

Figure 4 shows the fitted parameters using the Student's t distribution in each of the 40 slices versus the true mass. As can be seen in Figs. 4(a) and (b), the values of ν and λ exhibit a non-negligible dependence on the true mass, and these are fitted with a linear function. A linear fit was also carried out for the central value of the response function, μ, which showed that the values are to high accuracy consistent with zero. Therefore in the following we constrain μ to be zero.

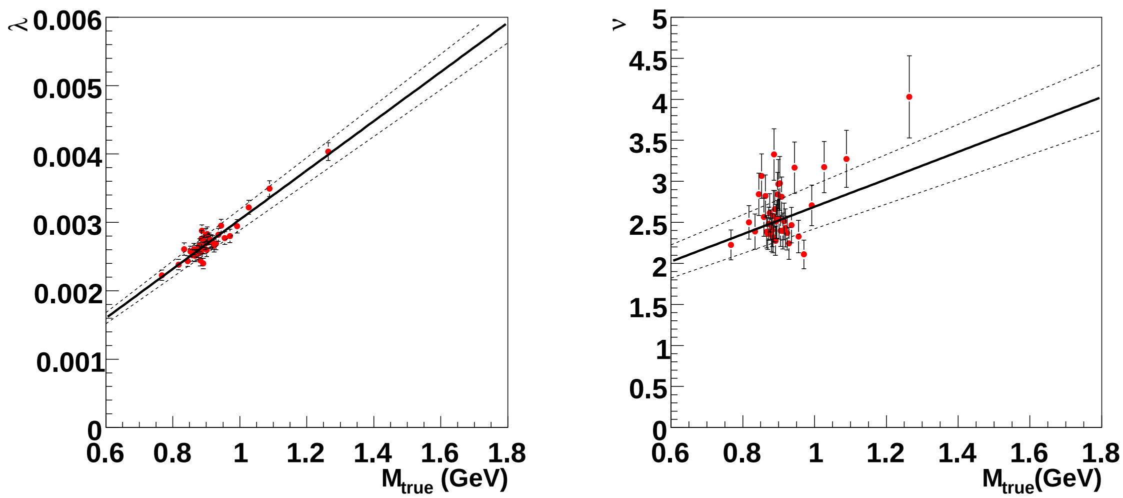

(a) (b)

Figure 4: Fitted parameter values of (a) the scale parameter λ and (b) the number of degrees of freedom ν of the Student's t distribution, versus true mass. The dashed lines indicated the variations in parameter values which were employed to assess systematic uncertainties.

The fitted values of ν and λ as a function of the true mass are then used to obtain the response matrix element R_{ij} for all values of the measured and true mass (i.e., all i and j) using

$$
\begin{aligned}
R_{ij} &= P(\text{found in bin } i\,|\text{true value in bin } j) \\
&= P(\text{found in bin } i\,|\text{found somewhere}) P(\text{found somewhere}|\text{true value in bin } j) \\
&= \int_{\text{bin}\, i} f(x; \vec{\theta}(m_{\text{true},j}))\, dx\, \varepsilon_j \ ,
\end{aligned}
\tag{18}
$$

where ε_j is the efficiency for bin j and $\vec{\theta} = (\lambda, \nu)$ represents the set of parameters that were fitted using the distributions of x from the individual slices.

5.3 Maximum-Likelihood fit

For our primary analysis we use a binned extended Maximum-Likelihood fit, where the number of events n_i in bin i is modeled as a Poisson distributed quantity.

The analysis requires the expected background given by the parameters β_i in (3). These are obtained from Monte Carlo, and thus their estimated values have a statistical error. In a least-squares fit, these errors can be taken into account by modifying the denominator of the expression to be minimised (see Section 5.4). In a binned maximum-likelihood fit, this is not possible. A method to include the statistical uncertainty arising from using finite MC samples was proposed by Barlow and Beeston [12], which was adapted to our problem. Strictly speaking one should use a binomial model for m_{ij}, but we approximate m_{ij} as a Poisson variable because the number of background events in each bin for each component is small compared to the total number of generated MC events.

For a given background component j, for each bin i, let the expected number of events be β_{ij}. The Monte Carlo sample for this background mode gives a number of events m_{ij} observed in the corresponding bin. The expectation value of m_{ij} is related to β_{ij} by

$$E[m_{ij}] = \tau_j r_j \beta_{ij} , \tag{19}$$

where τ_j is a scale factor that relates the luminosity of the MC sample for mode j to that of the data, and r_j is a factor that allows for the uncertainty in the prediction of the rate of the background process. The best estimate of r_j is equal to unity, but this is treated as a Gaussian distributed quantity with a standard deviation equal to the relative uncertainty on the production rate for the jth background mode.

The uncertainties in the values of other nominally fixed model parameters, e.g., the resonance parameters of the K*(1410), can be incorporated into the fit in a similar way. For a given parameter η one has a previously estimated value $\hat{\eta}$ and standard deviation σ_η, taken, e.g., from the PDG. One includes in the likelihood function a Gaussian term in η centered about $\hat{\eta}$ with a standard deviation σ_η, and regards η as an adjustable parameter. In the nominal fit presented below, this procedure is applied only for the mass and width of the K*(1410) (referred to below as η_1 and η_2).

We also include in the likelihood function terms which account for the uncertainty in the shapes of background mass distributions. From Fig. 7(a) one can see that the contributions from tau-lepton decays to $K^0_S\pi^-K^0_L$ and $K^0_S\pi^-\pi^0$ both have a peaking structure at the mass of the K*(892), and thus any uncertainty in the modeling of these modes will lead to a systematic uncertainty in the measurement of the K*(892) mass and width. This is particularly true for the $K^0_S\pi^-K^0_L$ mode, as it makes a larger contribution and the information on its shape is based largely on lower-statistics measurements from LEP. The mass and width of the K*(892) for the MC simulation of this mode were taken to be the nominal PDG values, which differ by about 3 and 5 MeV, respectively, from the values found in the present analysis. Therefore we assign a 3 MeV uncertainty to the mean and 5 MeV uncertainty to the width of the $K^0_S\pi^-K^0_L$ background contribution.

To propagate these uncertainties into the full fit of the $K^0_S\pi^-$ mass distribution, we introduce two additional adjustable parameters, $\vec{\alpha} = (\alpha_1, \alpha_2)$, which have the effect of shifting and stretching the shape of the distribution. This transformation is applied to the β_{ij} values for the $K^0_S\pi^-K^0_L$ background mode and the altered values are then used in the likelihood function. The mean and standard deviation of the initial MC template are prevented from changing too much by regarding their nominal values as Gaussian distributed estimates with the assigned uncertainties of $\sigma_{\mu_{KK\pi}} = 3\,\text{MeV}$ and $\sigma_{\sigma_{KK\pi}} = 5\,\text{MeV}$, respectively. More details on the mathematical procedure are given in Ref. [13].

Applying this procedure to the $K^0_S\pi^-K^0_L$ background mode led to very small increases in the errors of the mass and width of the K*(892). As the next largest background contribution from $K^0_S\pi^-\pi^0$ is substantially smaller and furthermore its shape was directly measured specifically for use in the present analysis, the effect of its systematic uncertainty is not considered to make a significant contribution. Therefore we only include the extra parameters α_1 and α_2 for the $K^0_S\pi^-K^0_L$ background.

Putting together these ingredients we can write the full likelihood function as the following product of Poisson terms for n_i and m_{ij} and Gaussian terms for r_j, the mass and width of the K*(1410), and for the mean and standard deviation of the $K^0_S\pi^-K^0_L$ background:

$$\begin{aligned}
L(\mu_{\rm tot},\vec{\theta},\vec{\beta},\vec{r},\vec{\eta},\vec{\alpha}) &= \prod_{i=1}^{N}\frac{\nu_i^{n_i}}{n_i!}e^{-\nu_i}\times\prod_{i=1}^{N}\prod_{j=1}^{N_{\rm bkg}}\frac{(\tau_j r_{ij}\beta_{ij})^{m_{ij}}}{m_{ij}!}e^{-\tau_j r_{ij}\beta_{ij}} \\
&\times \prod_{j=1}^{N_{\rm bkg}}\frac{1}{\sqrt{2\pi}\sigma_{r_j}}e^{-(r_j-1)^2/2\sigma_{r_j}^2} \\
&\times \prod_{k}\frac{1}{\sqrt{2\pi}\sigma_{\eta_k}}\exp\left(-\frac{1}{2}\frac{(\eta_k-\hat{\eta}_k)^2}{\sigma_{\eta_k}^2}\right) \\
&\times \frac{1}{\sqrt{2\pi}\sigma_{\mu_{KK\pi}}}\exp\left(-\frac{1}{2}\frac{(\mu_{KK\pi}(\vec{\alpha})-\mu_{KK\pi}(0))^2}{\sigma_{\mu_{KK\pi}}^2}\right) \\
&\times \frac{1}{\sqrt{2\pi}\sigma_{\sigma_{KK\pi}}}\exp\left(-\frac{1}{2}\frac{(\sigma_{KK\pi}(\vec{\alpha})-\sigma_{KK\pi}(0))^2}{\sigma_{\sigma_{KK\pi}}^2}\right) . \qquad (20)
\end{aligned}$$

Here $\mu_{KK\pi}(0)$ and $\sigma_{KK\pi}(0)$ are the nominal mean and standard deviation of the $K^0_S\pi^-K^0_L$ background, and $\mu_{KK\pi}(\vec{\alpha})$ and $\sigma_{KK\pi}(\vec{\alpha})$ are the values corresponding to the parameters $\vec{\alpha}=(\alpha_1,\alpha_2)$. The parameters $\mu_{\rm tot}$, $\vec{\theta}$, $\vec{\beta}$ $\vec{r}$ and $\vec{\alpha}$ enter through equations (3), (6) and (19).

Instead of maximizing L we minimize the equivalent quantity proportional to $-2\ln L$, normalized in such a way that the minimized value behaves like a chi-square distributed goodness-of-fit statistic (see, e.g., [9]):

$$\begin{aligned}
\chi^2(\mu_{\rm tot},\vec{\theta},\vec{\beta},\vec{r},\vec{\eta},\vec{\alpha}) &= 2\sum_{i=1}^{N} n_i\ln\frac{n_i}{\nu_i(\vec{\theta})}+\nu_i(\vec{\theta})-n_i \\
&+ 2\sum_{i=1}^{N}\sum_{j=1}^{N_{\rm bkg}} m_{ij}\ln\frac{m_{ij}}{\tau_j r_{ij}\beta_{ij}}+\tau_j r_{ij}\beta_{ij}-m_{ij} \\
&+ \sum_{j=1}^{N_{\rm bkg}}\left(\frac{r_j-1}{\sigma_{r_j}}\right)^2+\sum_k\left(\frac{\eta_k-\hat{\eta}_k}{\sigma_{\eta_k}}\right)^2 \\
&+ \left(\frac{\mu_{KK\pi}(\vec{\alpha})-\mu_{KK\pi}(0)}{\sigma_{\mu_{KK\pi}}}\right)^2+\left(\frac{\sigma_{KK\pi}(\vec{\alpha})-\sigma_{KK\pi}(0)}{\sigma_{\sigma_{KK\pi}}}\right)^2 . \qquad (21)
\end{aligned}$$

In Eq. (21) the logarithmic terms are taken as zero if the observed number of events (n_i or m_{ij}) is zero. It can be shown that for all n_i and m_{ij} sufficiently large, the sampling distribution of of this quantity approaches a chi-square distribution for $N_{\rm meas} - n_{\rm par}$ degrees of freedom, where $N_{\rm meas}$ is the number of measured values and $n_{\rm par}$ is the number of adjustable parameters. Only a few of the bins in the measured distribution have less than 10 entries, and therefore the minimized value of (21) provides a measure of goodness-of-fit that is to good approximation equivalent to the usual chi-square statistic.

To determine the number of degrees of freedom, not only the n_i but also the m_{ij} count effectively as measured values, as do the estimated of values of unity for each of the r_j, the nominal K*(1410) mass, and the nominal values of the mean and standard deviation of the $K^0_S\pi^-K^0_L$ background. Thus the inclusion of the parameters β_{ij}, r_j, η_1, η_2, α_1 and α_2 are compensated by corresponding values that are treated as measurements and there is no resulting change in the number of degrees of freedom; for the nominal fit this is 88.

5.4 Least-Squares fit

It is useful to also perform a Least-Squares(LS) fit to the data which can serve as an important cross-check of our final parameter values. Each of the background components is subtracted from the data, yielding measured values

$$y_i = n_i - \sum_j \frac{m_{ij}}{r_j \tau_j} \tag{22}$$

where r_j and τ_j are defined in Section 5.3 above. The expected number of events is found (cf. equation (3)) using

$$\lambda_i = \sum_j R_{ij} \mu_j \ . \tag{23}$$

We then minimize

$$\begin{aligned} \chi^2(\mu_{\rm tot}, \vec{\theta}, \vec{r}, \vec{\eta}, \vec{\alpha}) \quad = \quad & \sum_{i=1}^{N} \frac{(y_i - \lambda_i)^2}{{\sigma_i}^2} + \sum_{j=1}^{N_{\rm bkg}} \left(\frac{r_j - 1}{\sigma_{r_j}} \right)^2 + \sum_k \left(\frac{\eta_k - \hat{\eta}_k}{\sigma_{\eta_k}} \right)^2 \\ + \quad & \left(\frac{\mu_{KK\pi}(\vec{\alpha}) - \mu_{KK\pi}(0)}{\sigma_{\mu_{KK\pi}}} \right)^2 + \left(\frac{\sigma_{KK\pi}(\vec{\alpha}) - \sigma_{KK\pi}(0)}{\sigma_{\sigma_{KK\pi}}} \right)^2 \ , \end{aligned} \tag{24}$$

where σ_i^2 is the estimated value of the variance of y_i. This is given by

$$V[y_i] = V\left[n_i - \sum_j \frac{m_{ij}}{r_j \tau_j} \right] = V[n_i] + \sum_j \left(\frac{1}{r_j \tau_j} \right)^2 V[m_{ij}] \tag{25}$$

For the denominator used in the LS fit this can be estimated by

$$\sigma_i^2 = n_i + \sum_j \left(\frac{1}{r_j \tau_j} \right)^2 m_{ij} \ . \tag{26}$$

5.5 FIT RESULTS FOR $K_S^0\pi^-$ MASS DISTRIBUTION

The fitting procedures described above have been carried out using a variety of hypotheses. Figures 5 to 7 show our Least-Squares fits, while Figure 8 is performed using the method of Maximum-Likelihood.

(a) single K*(892)

(b) K*(892) + K*(1410)

(c) K*(800) + K*(892) + K*(1410)

(d) K*(800) + K*(892) + K*(1430)

(e) K*(800) + K*(892) + K*(1680)

(f) K*(892) + LASS

Results for the fits are shown in Figs. 5 through 8 and in Table 4. As described earlier the fitted r parameters,(and α_1,α_2 for the $K_S^0K_L^0\pi^-$) determine a new shape for the background, and it is this new background shape which is subtracted from the data. As such each background subtracted data histogram will look different for each fit.

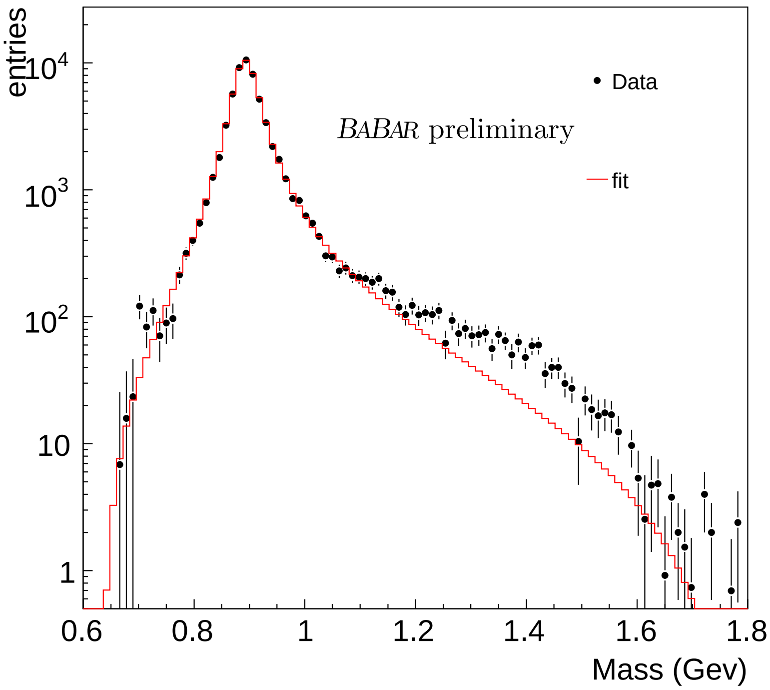

(a)

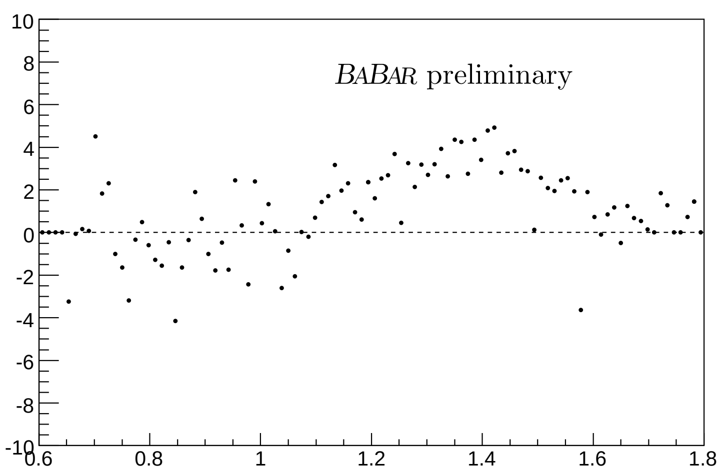

(b)

Figure 5: (a) $K_S^0\pi^-$ invariant mass distribution fit using only the K*(892) resonance, and (b) the measured minus fitted values divided by the measurement errors

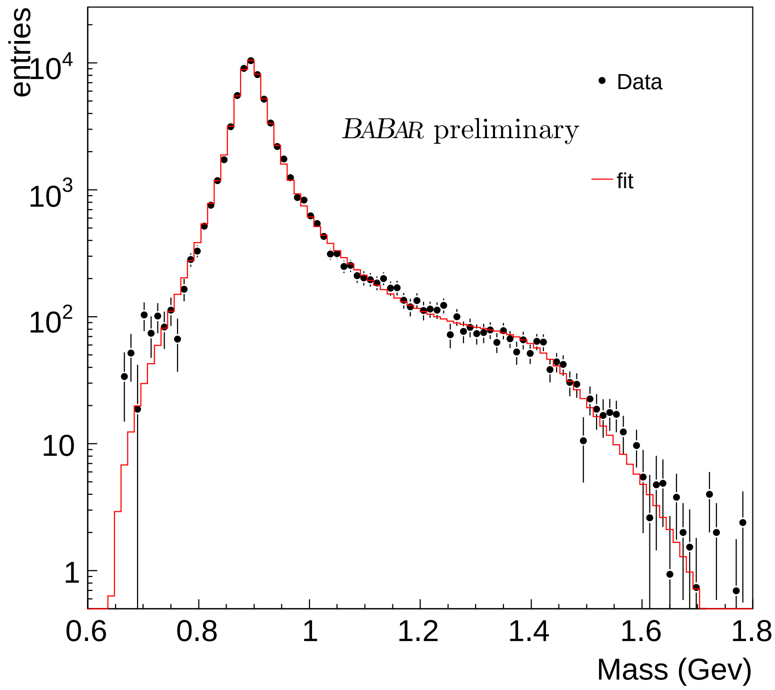

(a)

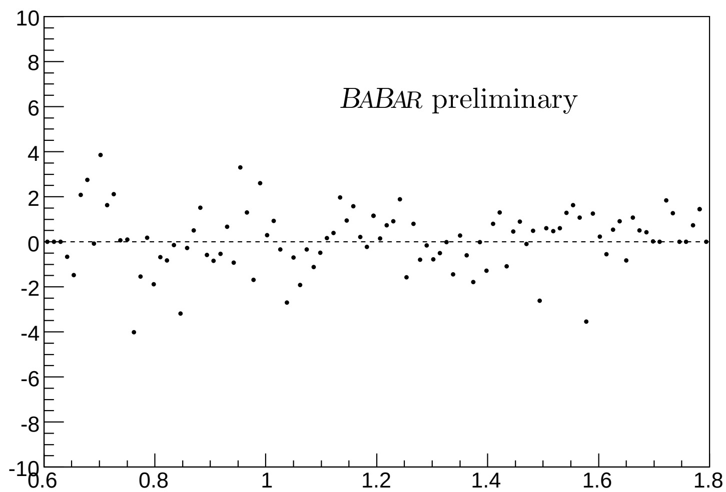

(b)

Figure 6: (a)$K_S^0\pi^-$invariant mass distribution fit using a K*(892) + K*(1410),and (b) the measured minus fitted values divided by the measurement errors

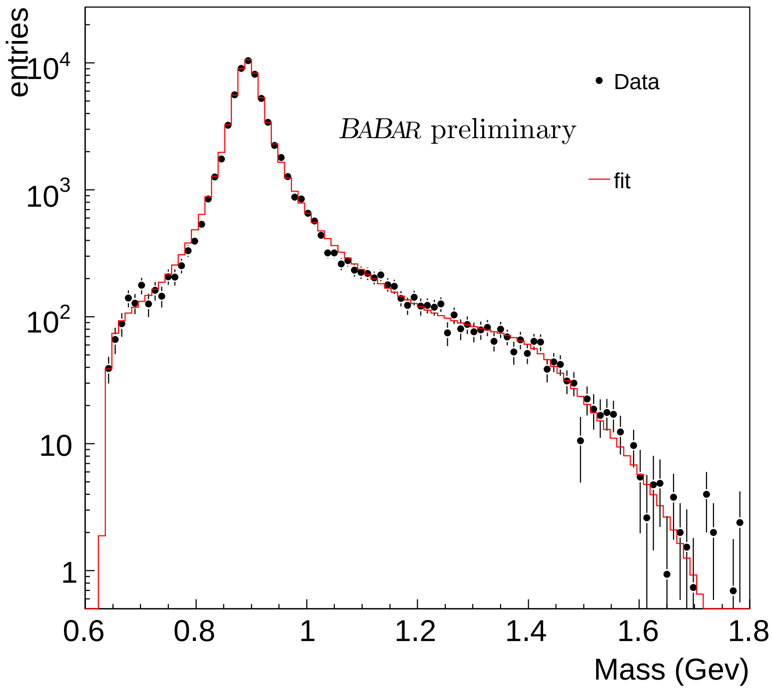

(a)

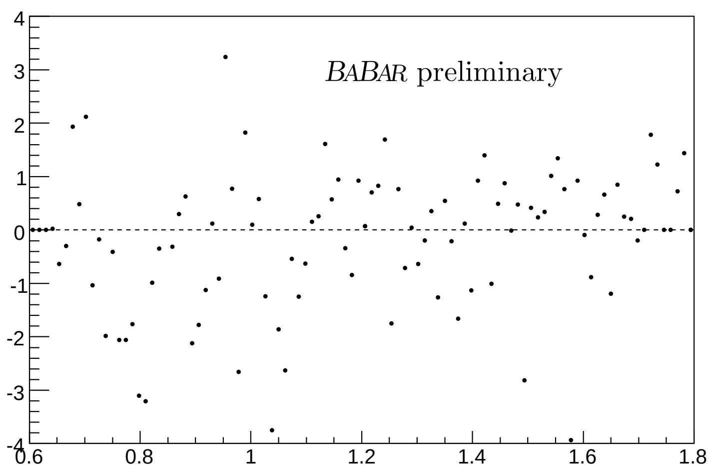

(b)

Figure 7: (a) $K_S^0\pi^-$invariant mass distribution fit using K*(800) + K*(892) + K*(1410), and (b) the measured minus fitted values divided by the measurement errors

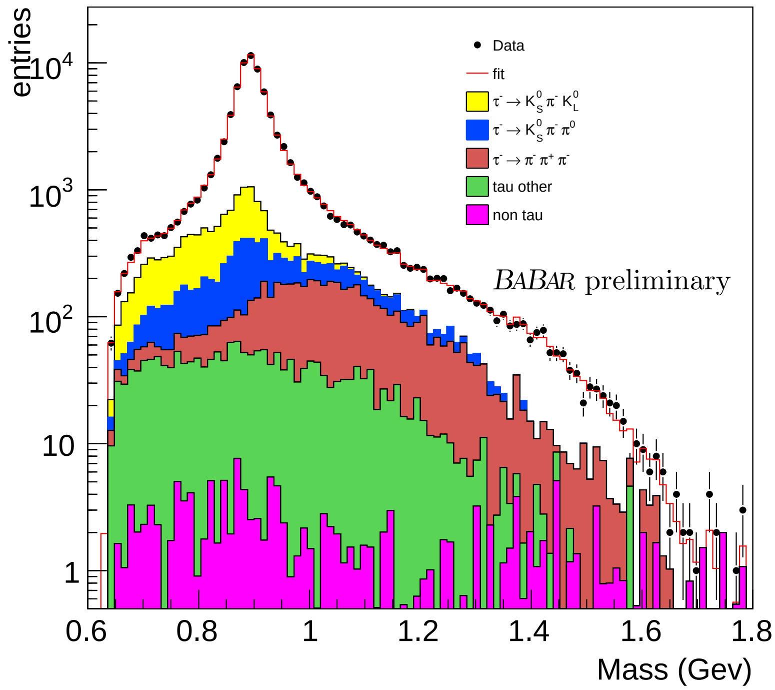

(a)

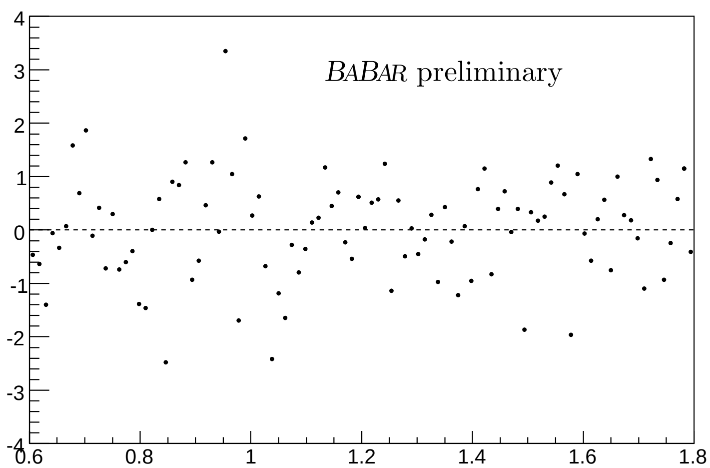

(b)

Figure 8: (a) Fit of $K_S^0\pi^-$ invariant mass distribution without background subtracted, using K*(892) and K*(1410) and K*(800),and (b) the measured minus fitted values divided by the measurement errors. The method of maximum likelihood is used to perform this fit.

5.5.1 Discussion of fits

Figure 5(a) shows that a single K*(892) is clearly not enough to model the mass spectrum accurately. This was seen by the Belle collaboration [3], which proposed that the distribution should contain contributions from a K*(800) scalar and K*(1410) vector resonances.

In the region around 1.4 GeV in Fig. 5(a), the data are significantly higher than the fitted curve. As can be seen in Fig. 6, the addition of the K*(1410) gives a significant improvement to the high mass region, yielding a χ^2 of 130.04 for 95 degrees of freedom. In these fits the rate of the K*(1410) was allowed to vary within the error given in the PDG.However, to enable this two-resonance fit model to accurately fit the low mass region, the background in this area has to be distorted. This can be seen by the fitted r values from our model, shown in Table 3. Columns (a) and (b) show the values for our one resonance and two resonance models.The default value of r is 1 for all background modes; where r is less than 1 indicates that the fit has had to increase the rate of this mode by a factor $1-r$. This is especially prominent in the $\tau \to K^0_S K^0_L \pi^- \nu_\tau$ mode.

The inclusion of the K*(800) further reduces our χ^2 to 113.05 for 94 degrees of freedom. This is a significantly better goodness-of-fit value than our K*(892) + K*(1410) fit model. For the mass and width of the K*(800) we use the measurements from the BES collaboration [14]. The result is shown in Fig. 7(a). In addition the r values for this fit, shown in column (c) in Table 3, are closer to 1, indicating the fit is not having to vary these backgrounds by much to fit the total mass spectrum. This can also be seen by considering the background in the low mass region in Figs. 5(a) to 7(a)., where there is significantly less background in the one and two resonance fits compared to the fit including the K*(800).

Table 3: Table of fitted r parameters(see text).Column (a) refers to a fit using only a K*(892), column (b) refers to a fit using K*(892) + K*(1410) and column (c) refers to a fit using K*(800) + K*(892) + K*(1410).

	(a)	(b)	(c)
$\tau \to K^0_S K^0_L \pi^- \nu_\tau$	0.852±0.034	0.773±0.030	1.134±0.078
$\tau \to K^0_S \pi^- \pi^0 \nu_\tau$	0.977±0.050	1.00754±0.047	1.037±0.046
$\tau \to \pi^+ \pi^- \pi^- \nu_\tau$	0.982±0.0086	0.9998±0.0088	1.0008±0.0088
$\tau \to$ other	0.953±0.033	0.986±0.033	0.995±0.032
non τ background	1.00000	1.00000	1.00000

The $\tau \to K^0_S K^0_L \pi^- \nu_\tau$ mode is based on Monte Carlo form factors derived from a low statistics ALEPH measurement [15]. It is therefore plausible that this is not an accurate representation of the shape of this mode. In order to ascertain by how much the $\tau \to K^0_S K^0_L \pi^- \nu_\tau$ background would have to vary to completely account for the low mass shoulder, in the absence of a K*(800), we repeated the fit with a K*(892) + K*(1410) and removed the penalty term for the mean and standard deviation of the $\tau \to K^0_S K^0_L \pi^- \nu_\tau$ background in the χ^2 minimisation. This would enable the fit to have a larger parameter space in which to find the minimum. The result of this fit yields a χ^2dof = 115.7/92 which is very close to our nominal fit value, which indicates that this model can in principle provide a good description of the data. However the $\tau \to K^0_S K^0_L \pi^- \nu_\tau$ has to be distorted by a significant amount, which can be seen in Figure 9(a). It should be noted that when one considers the mass spectrum obtained by ALEPH, it exhibits large experimental uncertainties, and therefore our distorted histogram is reasonably consistent with the ALEPH result [15]. It is therefore not possible at this stage to comment firmly on the existence or necessity of a K*(800) in our mass spectrum. Further studies on the mass spectrum of the $\tau \to K_S^0 K_L^0 \pi^- \nu_\tau$ background mode are ongoing to confirm that the Monte Carlo is accurate.

If instead of a K*(1410) one uses a scalar K*(1430), one finds a comparable χ^2 value of 114.11 for 94 degrees of freedom. As such the K*(1410) and K*(1430) cannot be differentiated on their χ^2 value.

Using the LASS function for the scalar form factor gives a χ^2 value of 157.7 for 94 degrees of freedom, i.e., significantly worse than our nominal fit.

We also present a fit using the K*(1680) instead of the K*(1410), as a check of the similar exercise carried out by Belle. Using only this resonance for the high-mass region, however, does not provide an adequate description of the data.

To summarize, the fit using only the two resonances K*(892) and K*(1410) is able to describe the low-mass region of the distribution,if the modeling of the background were to be wrong by a significant amount. This is currently being investigated. The model using K*(800) + K*(892) + K*(1410) gives the best goodness-of-fit based on the χ^2 value, and so this is chosen to be our preliminary nominal fit. The difference between the parameter values of these two fit models are used as systematic uncertainties. This is discussed further in the next section. The resulting values for the mass and width of the K*(892) are found to be

$$M(K^*(892)^-) = 894.57 \pm 0.19\,(\text{stat.})\,\text{MeV}\,, \tag{27}$$

$$\Gamma(K^*(892)^-) = 45.89 \pm 0.43\,(\text{stat.})\ .\text{MeV} \tag{28}$$

The statistical errors quoted already cover a number of systematic uncertainties such as those in the rates and shapes of backgrounds, which were incorporated by including corresponding adjustable parameters in the fit. Several additional sources of systematic uncertainty are discussed in Section 5.6.

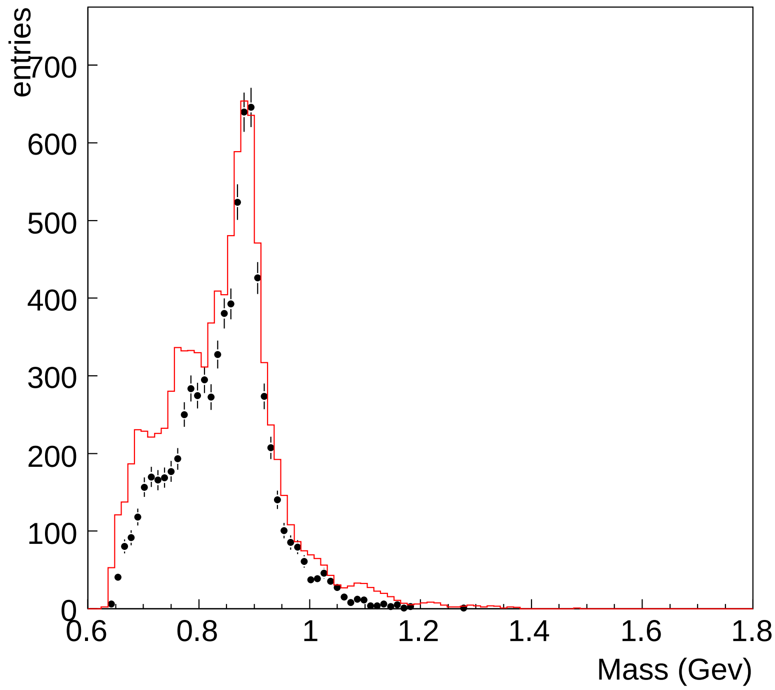

(a)

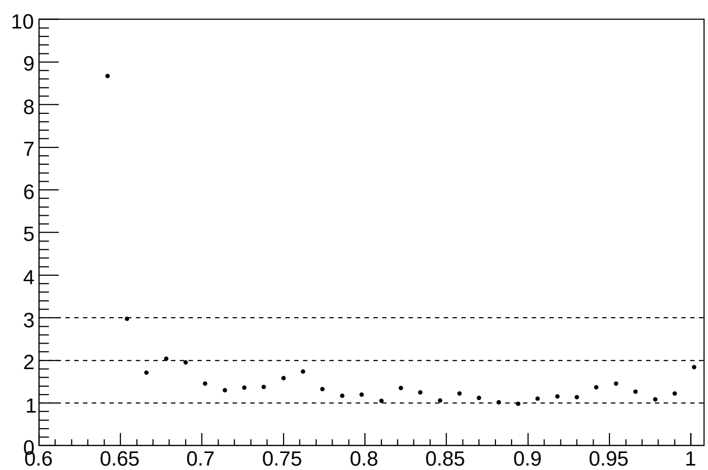

(b)

Figure 9: (a)The original Monte Carlo histogram for $\tau \to K_S^0 K_L^0 \pi^- \nu_\tau$ (points), and the distortion needed to account for the low mass shoulder (red line).(b) The ratio of the distorted histogram to the Monte Carlo histogram for the low mass shoulder.

Table 4: Table of Fitted parameters: The inclusion of different resonances are denoted by the symbol $\oplus$. Square brackets [ ] around the paramters denote that they have been fixed in the fit. Curly brakets { } around the parameters denote that they have been constrained in the fit. Column c is the nominal fit

Scenario	a	b	c	d	e	f
Resonances	K*(892) $\oplus$	K*(892) $\oplus$ [K*(1410)]	[K*(800)] $\oplus$ K*(892) $\oplus$ {K*(1410)}	[K*(800)] $\oplus$ K*(892) $\oplus$ [K*(1430)]	[K*(800)] $\oplus$ K*(892) $\oplus$ [K*(1680)]	K*(892)$\oplus$ LASS
$M(892)$ (MeV/c^2)	894.544±0.171	894.412±0.187	894.565±0.193	894.673±0.193	894.393±0.184	894.855±0.196
$\Gamma(892)$ (MeV)	47.673±0.437	46.206±0.455	45.893±0.434	45.834±0.426	45.491±0.392	47.022±0.452
$\|\beta\|$	N/A	0.095±0.006	0.075±0.007	N/A	N/A	
$\arg(\beta)$	N/A	1.983±0.139	1.747±0.18	N/A	N/A	
$M(1410)$ (MeV/c^2)	N/A	{1434.23±11.19 (PDG)}	{1425.55±12.47 (PDG)}	N/A	N/A	N/A
$\Gamma(1410)$ (MeV)	N/A	{253.80±17.68 (PDG)}	{238.76±18.85 (PDG)}	N/A	N/A	N/A
$\|\lambda\|(1430)$	N/A	N/A	N/A	5.059±0.311		N/A
$\arg(\lambda)(1430)$	N/A	N/A	N/A	8.670±0.244		N/A
$M(1430)$ (MeV/c^2)				[1425±50(PDG)]		
$\Gamma(1430)$ (MeV)				[270±80(PDG)]		
$\|\gamma\|(1680)$					0.199±0.016	
$\arg(\gamma)(1680)$					3.559±0.184	
$M(1680)$ (MeV/c^2)	N/A	N/A	N/A	N/A	[1717±27 (PDG)]	
$\Gamma(1680)$ (MeV)	N/A	N/A	N/A	N/A	[322±110 (PDG)]	
$M(800)$ (MeV/c^2)	N/A	N/A	[841±30$^{+81}_{-73}$ (BES)]	[841±30$^{+81}_{-73}$ (BES)]	[841±30$^{+81}_{-73}$ (BES)]	
$\Gamma(800)$ (MeV)	N/A	N/A	[618±90$^{+96}_{-144}$ (BES)]	[618±90$^{+96}_{-144}$ (BES)]	[618±90$^{+96}_{-144}$ (BES)]	
$\varkappa$	N/A	N/A	1.938±0.11	0.255±0.019	2.237±0.101	
χ^2	399.778	130.044	113.049	119.108	144.711	148.375
# d.o.f.	97	95	94	94	94	94
χ^2/# d.o.f.	4.121	1.369	1.203	1.267	1.539	1.579
Prob.(χ^2)	<0.0001	0.0098	0.0880	0.0411	0.0006	0.0002

5.6 SYSTEMATIC UNCERTAINTIES

Several important sources of systematic uncertainty are already covered in the fit by including in the model corresponding adjustable parameters, as described in Section 5.3. These include the uncertainty due to limited Monte Carlo statistics, total background rates, and the shape of the $K_S^0\pi^-K_L^0$ background.

Two additional sources of systematic uncertainty in the $\tau^- \to K_S^0\pi^-\nu_\tau$ analysis are from the response matrix and the choice of fit model. These are discussed in Sections 5.6.1 – 5.6.2 below and summarized in Section 5.6.3.

5.6.1 Uncertainty in the response matrix

The response matrix R_{ij} is derived from the Monte Carlo simulation of the detector. As described in Section 5.2, the response matrix was parameterized using a Student's t distribution with an adjustable scale parameter λ and number of degrees of freedom ν, each of which were themselves fitted as a linear function of the true hadronic mass.

As a conservative estimate of the uncertainty of the detector response, which is dominated by modeling of the tracking and Calorimeter, we have varied λ by $\pm 5\%$ and ν by $\pm 10\%$ relative to its nominal fitted value. Varying λ results in a 0.18 MeV change in the width of the K*(892) and a 0.023 MeV change in the mass. Varying ν results in a 0.28 MeV change in the width of the K*(892) and a 0.030 MeV change in the mass.

5.6.2 Uncertainty due to choice of fit model

As a check of the fitting method we have taken a fully reconstructed Monte Carlo sample of signal events, and fitted them using the signal model. As the MC generator models the $\tau^- \to K_S^0\pi^-\nu_\tau$ decay with only the K*(892) resonance, the fit model also only contained this resonance. The fit gives values for the mass and width of the K*(892) of

$$\begin{aligned} M(K^*(892)^-) &= 891.924 \pm 0.143\,(\text{stat.})\,, \\ \Gamma(K^*(892)^-) &= 51.138 \pm 0.326\,(\text{stat.})\,. \end{aligned}$$

The K*(892) mass and width values in the generator are

$$\begin{aligned} M(K^*(892)^-) &= 891.660\,, \\ \Gamma(K^*(892)^-) &= 50.800\,. \end{aligned}$$

The difference between the input and fitted values are 0.264 MeV and 0.338 MeV for the mass and width respectively. We take this difference and apply a correction as an additive shift in our nominal values. This changes our nominal fit values to 894.301 MeV and 45.555 Mev for the mass and width respectively of the K*(892). The statistical errors on each parameter are then taken as systematic uncertainties and are added in quadrature to the other systematic uncertainties.

A further uncertainty in the fit model stems from the choice of resonances to include in the fit. Although using the K*(1430) instead of the K*(1410) resulted in a small increase in the χ^2, the model provides nevertheless a good qualitative fit to the data. The fit model which uses just a K*(892) and K*(1410) is also able to provide a good fit, albeit with a significantly distorted background. Therefore we take the difference in the mass and width values for the K*(892) between our nominal fit and the alternative models which also yield comparable χ^2 values, as a source of systematic uncertainty. The largest discrepancy in parameter values came from our two resonance model, which yielded K*(892) mass and width values of 894.447 MeV and 46.223 MeV respectively. The results of our systematic studies are summarized in Table 5.

5.6.3 Summary of systematic uncertainties

Table 5 summarizes the systematic uncertainties for the fit of the measurements of the mass and width of the K*(892).

Table 5: Table of systematic uncertainties in the mass and width of the K*(892) (see text).

	M(K*(892))	Γ(K*(892))
Response matrix width (±5% variation of λ)	0.023	0.180
Response matrix tails (±10% variation of ν)	0.030	0.280
Statistical error on fit to reconstructed MC	0.143	0.326
Without using K*(800)	0.118	0.330
Total systematic (quadratic sum)	0.189	0.571

6 SUMMARY AND CONCLUSIONS

We have carried out studies of the decays $\tau^- \to K^0_S\pi^-\nu_\tau$ and $\tau^- \to K^0_S\pi^-\pi^0\nu_\tau$ using 384.6 fb^{-1} of e^+e^- collision data provided by the PEP-II accelerator, operating primarily at $\sqrt{s} = 10.58\,\mathrm{GeV}$, and recorded using the *BABAR* detector. We have measured the branching ratios for $\tau^- \to K^0_S\pi^-\pi^0\nu_\tau$, which is found to be

$$\mathcal{B}(\tau^- \to K^0\pi^-\pi^0\nu_\tau) = (0.342 \pm 0.006\,(\mathrm{stat.}) \pm 0.015\,(\mathrm{sys.}))\% .$$

The measurement of $\mathcal{B}(\tau^- \to K^0\pi^-\nu_\tau)$ is fully consistent with the preliminary result presented by the BaBar collaboration in 2008 [1]. It is also in good agreement with the value found by the Belle collaboration [3] and has a slightly smaller total uncertainty. For $\mathcal{B}(\tau^- \to K^0\pi^-\pi^0\nu_\tau)$ the value obtained is also consistent with the present world average and represents an improvement in accuracy by a factor of 2.

For the $\tau^- \to K^0_S\pi^-\pi^0\nu_\tau$ mode we have measured the mass distributions of different combinations of final state hadrons: $\pi^-\pi^0$, $K^0_S\pi^-$, $K^0_S\pi^0$ and $K^0_S\pi^-\pi^0$. These were used to make important improvements to the `TAUOLA` Monte Carlo generator, which allowed for a precise estimation of the background contribution from this mode in the analysis of the $\tau^- \to K^0_S\pi^-\nu_\tau$ channel.

We have carried out a fit of the hadronic mass distribution for $\tau^- \to K^0_S\pi^-\nu_\tau$. Including a systematic shift in our parameter values originating from an estimated reconstruction bias, (see section 5.6.2), this yields precise meausrements for the mass and width of the K*(892) resonance:

$$\begin{aligned} M(K^*(892)^-) &= 894.30 \pm 0.19\,(\mathrm{stat.}) \pm 0.19\,(\mathrm{syst.})\ \mathrm{MeV}\ , \\ \Gamma(K^*(892)^-) &= 45.56 \pm 0.43\,(\mathrm{stat.}) \pm .57\,(\mathrm{syst.})\ \mathrm{MeV}\ . \end{aligned}$$

These values confirm the Belle collaboration's measurements [3] that indicated a K*(892) mass several MeV higher and a width several MeV lower than the world average. The results reported here represent a factor of two improvement in accuracy relative to the Belle measurements.

We analyse the possiblity of other resonances being present in this mass spectrum, and conclude that a combination of K*(800), K*(892) and K*(1410) provides a good description of the data. A fit without the K*(800), i.e., using only a K*(892) + K*(1410) combination, can also provide a good description of the data if the modelling of the $\tau \to K_S^0 K_L^0 \pi^- \nu_\tau$ were to be incorrect by a significant amount.The shape and rate distortions necessary for a two resonance model to fit the data are however reasonably consistent with the large experimental uncertainties on the ALEPH data that was used in the generation of this background mode. As such further study is necessary on this mode and is ongoing.

Figure 10 shows the results of various measurements that went into calculating the 2007 PDG average values for the mass and width of the K*(892). The Belle 2007 result and our result both indicate a shift towards 895 MeV for the mass value.

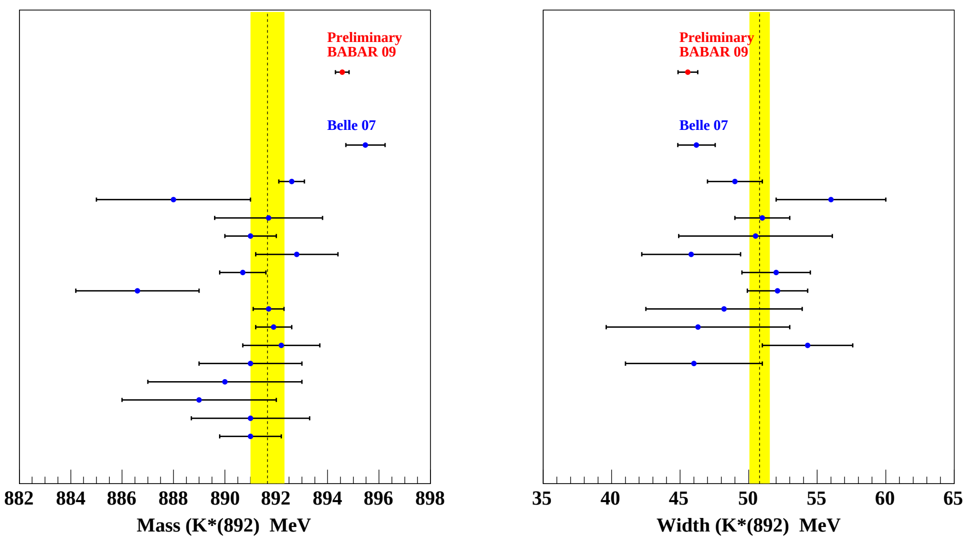

Figure 10: Comparison of the K*(892) mass and width values which were included in the PDG07 calculated average value and the recent result from Belle, and our result. The majority of the PDG07 values are from hydrogen bubble chamber experiments.

7 ACKNOWLEDGEMENTS

We are grateful for the extraordinary contributions of our PEP-II colleagues in achieving the excellent luminosity and machine conditions that have made this work possible. The success of this project also relies critically on the expertise and dedication of the computing organizations that support *BABAR*. The collaborating institutions wish to thank SLAC for its support and the kind hospitality extended to them. This work is supported by the US Department of Energy and National Science Foundation, the Natural Sciences and Engineering Research Council (Canada), the Commissariat à l'Energie Atomique and Institut National de Physique Nucléaire et de Physique des Particules (France), the Bundesministerium für Bildung und Forschung and Deutsche Forschungsgemeinschaft (Germany), the Istituto Nazionale di Fisica Nucleare (Italy), the Foundation for Fundamental Research on Matter (The Netherlands), the Research Council of Norway, the Ministry of Education and Science of the Russian Federation, Ministerio de Educación y Ciencia (Spain), and the Science and Technology Facilities Council (United Kingdom). Individuals have received support from the Marie-Curie IEF program (European Union) and the A. P. Sloan Foundation.

References

[1] B. Aubert *et al.*, *Measurement of* $\mathcal{B}(\tau^- \to K^0_S \pi^- \nu_\tau)$ *using the BaBar detector*, arXiv:0808.1121 (hep-ex);

[2] S. Jadach, Z. Was, R. Decker and J.H. Kühn, Comput. Phys. Commun. 76 (1993) 361.

[3] D. Epifanov *et al.* [Belle Collaboration], Phys. Lett. B **654**, 65 (2007) [arXiv:0706.2231 [hep-ex]].

[4] B. Aubert *et al.*, Nucl. Instrum. Meth. A479 (2002) 1.

[5] PEP-II: An asymmetric *B* Factory. Conceptual Design Report, 1993, SLAC-R-418.

[6] S. Banerjee *et al.*, Phys. Rev. Lett. D **77** (2008) 054012.

[7] B.F.L. Ward, S. Jadach and Z. Was, Nucl. Phys. Proc. Suppl. (2003) 73.

[8] W. M. Yao *et al.* [Particle Data Group], J. Phys. G **33**, 1 (2006).

[9] G. Cowan, Statistical Data Analysis, 1998 Oxford University Press.

[10] D. Aston et al., (LASS Collaboration) Nucl.Phys.B **296** (1988) 493.

[11] W.T. Eadie, D. Drijard, F.E. James, M. Roos and B. Sadoulet, *Statistical Methods in Experimental Physics*, North-Holland, Amsterdam (1971).

[12] Roger Barlow and Christine Beeston, *Fitting using finite Monte Carlo samples*, Comp. Phys. Comm. 77 (1993) 219–228.

[13] G. Cowan, *Increasing the flexibility of a distribution to allow for systematic uncertainty*, RHUL internal note, `www.pp.rhul.ac.uk/~cowan/stat/notes/AltHist.pdf` (2009).

[14] M. Ablikim *et al.* [BES Collaboration], Phys. Lett. B **633**, 681 (2006) [arXiv:hep-ex/0506055].

[15] R.Barate *et al*, Eur.Phys.J.C4:29-45,1998.